Indian Geotech J (December 2020) 50(6):1024–1040
https://doi.org/10.1007/s40098-020-00427-1

ORIGINAL PAPER

Investigations on Fracture Evolution of Coal Measure Sandstones from Mineralogical and Textural Points of View

Ekin Köken[1]

Received: 21 December 2019 / Accepted: 25 March 2020 / Published online: 9 April 2020

Abstract The purpose of the present study is to investigate the variations in fracture evolution of sandstones arising from mineralogical and textural features. For this purpose, eight types of coal measure sandstones located in the Zonguldak Hardcoal Basin (ZHB) were considered. The mineralogical and textural characterizations of the rocks were carried out. Physico-mechanical properties were determined for each rock type. Based on quantitative strain-based methods, the crack initiation (σ_{ci}) and crack damage (σ_{cd}) thresholds of the sandstones were determined. The laboratory test results indicate that the σ_{ci} and σ_{cd} of the sandstones were found to be between 0.27–0.43 and 0.61–0.83 of the UCS, respectively. In general, the σ_{ci} and σ_{cd} correspond to 0.37 and 0.71 of the UCS, respectively. The σ_{ci} and σ_{cd} decrease with increasing the sorting coefficient (S_c), average grain size (d_{50}, mm), contents of feldspar (F, %), and lithic fragment (LF, %). On the other hand, increasing quartz content (Qtz, %) increases those variables. Remarkable changes were obtained in the σ_{ci} and σ_{cd} when effective porosity (n_e) and pulse wave velocity (V_p) of the rocks exceed 3% and 3.00 km/s, respectively. As a result of mineralogical analyses and laboratory studies, statistical analyses were carried out. Accordingly, the σ_{ci} and σ_{cd} could be estimated reliably using several empirical relationships established in the present study. In order to represent the importance and utilization of rock mineralogy and texture for underground mining applications in the ZHB, several suggestions and considerations related to a V-cut gallery blasting operation were introduced.

✉ Ekin Köken
ekin.koken@agu.edu.tr

[1] Department of Materials Science and Nanotechnology Engineering, Abdullah Gül University, 38100 Kayseri, Turkey

Keywords Sandstone · Fracture evolution · Crack initiation · Crack damage · Mineralogical and textural analyses

Introduction

The mechanical behavior of rocks is of great importance to such investigations regarding open-pit and underground mining applications, tunneling, and extraction of natural resources such as coal, petroleum, natural gas, and hydrocarbons. In this respect, the fracture evolution of rocks stemming from drilling–blasting, excavation methods, and in situ stress states takes an important part in assessing the stability, reliability, and sustainability of those applications. Attempts to understand fracture mechanism around a rock mass have mainly involved laboratory investigations of rock materials, physical models as well as numerical analyses. On a theoretical basis, fracture evolution of rock materials under axial loading conditions is typically divided into four stages. These are crack initiation (1), crack propagation (2), unstable crack growth (3), and failure (4), each of which occurs at specific stress states [1, 2]. Crack initiation represents the stress level (σ_{ci}, MPa), where the first microfracture occurs in the rock itself. After the σ_{ci} has been reached, secondary cracks are initiated with progressive loading, which is called crack propagation. The crack damage stress (σ_{cd}, MPa) describes the point, where unstable crack growth commences followed by crack propagation. At the end of the σ_{cd}, fracture evaluation in a rock material ends up with a failure (Fig. 1).

Recently, the physical meaning and interpretation of stress state corresponding to crack initiation and damage have been investigated profoundly with a view to several

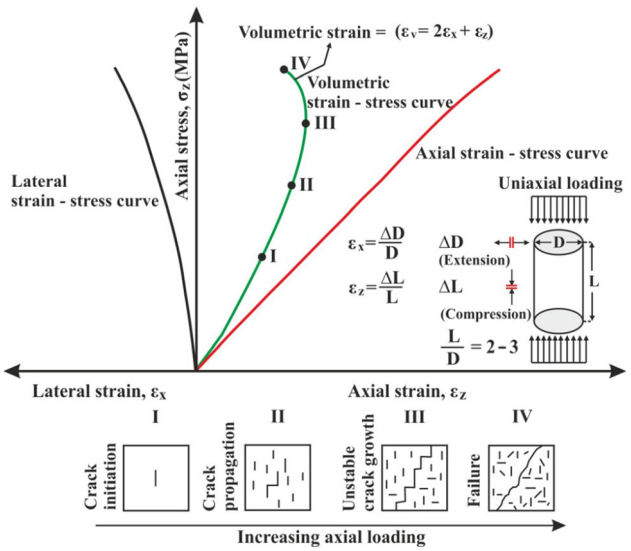

Fig. 1 Schematic representation of different stages of fracture evolution in a rock material under axial loading (modified after [1])

rock engineering approaches. The σ_{ci} was used in excavation damage and stability analyses of several rock masses [3–6]. Martin and Christiansson [7] suggested that the σ_{ci} could be drawn on estimations of the in situ spalling strength of crystalline rock masses. Damjanac and Fairhurst [8] pointed out that the σ_{ci} could also be utilized for the evaluation of long-term behavior of crystalline rocks.

Jiang et al. [9] performed several numerical analyses to investigate the effects of water jet applications on the fracture evolution of rocks. According to the numerical analyses, the researchers pointed out that crack initiation and propagation are key parameters to water jet applications. Lu et al. [10] indicated that controlling hydraulic fracturing and permeability of coal measure rocks could be possible with a branched tree-type borehole array whose performance has a link to crack initiation of rocks.

Liu et al. [11] expressed that higher values of σ_{ci} could give rise to lower penetration rates of tunneling boring machines (TBMs). Niu et al. [12] performed extensive research on sandstones that was focused on the variations in the σ_{ci} due to freezing–thawing (FT) cycles. The researchers demonstrated that the σ_{ci} decreased substantially due to progressive FT cycles. They consequently claimed that the variations in σ_{ci} values could be a complementary parameter in such rock engineering applications in cold regions.

The quantifications of σ_{ci} and σ_{cd} under axial loading are mainly conducted based on two different methods. The first method deals with stress–strain curves of rock materials, where axial (ε_z), lateral (ε_x), and volumetric strain ($\varepsilon_v = 2\varepsilon_x + \varepsilon_z$) has been regarded [1, 13–19].

The latter covers cumulative acoustic emission (CAE) counts varying throughout the axial loading [2, 20–24]. In general, the σ_{ci} and σ_{cd} are mainly defined as a function of uniaxial compressive strength (UCS, MPa) of rocks. Typical intervals of σ_{ci} and σ_{cd} are listed in Table 1. It was reported in such previous studies that a number of factors have influences on the σ_{ci} and σ_{cd}. The main factors are mineralogical and textural features, rock weathering, mechanical properties as well as loading conditions (i.e., uniaxial or triaxial loading).

Erişiş et al. [24] found that increasing the ground mass (Gm) in basaltic rocks results in an increase in the σ_{ci}. For igneous rocks, the increase in alkali feldspar (K-Feld.) minerals escalates the σ_{ci}, whereas those in plagioclase (Plg) and biotite (Bt) lower the σ_{ci} [25]. On the other hand, for sedimentary rocks (i.e., shale, calcareous shale, and argillaceous shale) cracks are initiated at higher stress levels when the carbonate content is greater than that of clay content (C_c) [25]. Basu and Mishra [27] found that increasing effective porosity (n_e, %) and rock weathering in granites lower the σ_{ci}.

Similar to what Nicksiar and Martin [25] stated, Ündül et al. [29] reported that the increase in the Bt quantities of andesitic rocks decreases the σ_{ci}. In addition, using mineral contents of Plg, amphibole (Amp), and Gm, the researchers determined a positive correlation between the ratio of (Plg + Amp)/Gm and the σ_{ci}.

Köken [31] demonstrated that textural features of limestones have effects on their stress–strain behaviors. Nicksiar and Martin [32] performed discrete element analyses to investigate factors affecting crack initiation in low-porosity crystalline rocks and concluded that the sorting degree of grains in the rock samples modeled has enormous impacts on the peak and crack initiation stresses. For dolomitic rocks, the increase in grain size and porosity also cause a decrease in the σ_{ci} [33]. However, increasing grain size in granitic rocks has enormous impacts on the σ_{cd} rather than the σ_{ci} [34]. Backers and Stephansson [35] and Haeri et al. [36] reported that crack propagation has a link to K_{II} type fracture toughness as a mechanical property. The σ_{ci} and σ_{cd} were also investigated by triaxial compression tests [19, 37–39]. Accordingly, the σ_{ci} increases remarkably in parallel with confining pressure (σ_3, MPa).

The above-mentioned studies put into different perspectives on the applicability and importance of crack initiation and propagation for issues relating to rock engineering practices. The present study aims to explore the fracture evolution of the coal measure sandstones located in the Zonguldak Hardcoal Basin (ZHB, Zonguldak/Turkey) under axial loading conditions. Eight types of coal measure sandstones with different textural and mineralogical features were considered. Mineralogical and textural features of the sandstones were explored by different quantitative approaches.

Table 1 Typical values of σ_{ci} and σ_{cd} under uniaxial compression for several rock types

Rock type	σ_{ci}/UCS	σ_{cd}/UCS	UCS (MPa)	References
Diorite	0.35–0.56 (0.49)[a]	NR–NR (NR)	171–294 (227)	[17]
Granite	0.47–0.59 (0.51	NR–NR (NR)	112–157 (137)	[18]
Siltstone	0.33–0.59 (0.43)	0.63–0.90 (0.77)	96–142 (131)	[19]
Various igneous rocks	0.43–0.50 (0.48)	0.64–0.90 (0.76)	143–225 (177)	[20]
Sandstone	0.31–0.54 (0.41)	NR–NR (NR)	72–104 (86)	[23]
Granite	0.32–0.65 (0.43)	NR–NR (NR)	102–124 (116)	
Basalt	0.33–0.54 (0.41)	0.83–0.98 (0.92)	145–271 (206)	[24]
Various rock types	0.42–0.47 (0.45)	NR–NR (NR)	15–371 (178)	[25]
Granite	0.42–0.62 (0.44)	0.65–0.94 (0.79)	129–157 (146)	[26]
Granite with different weathering grades	0.18–0.58 (0.38)	NR–NR (NR)	80–184 (143)	[27]
Granite	0.49–0.53 (0.51)	0.62–0.79 (0.71)	166–198 (178)	[28]
Andesite	0.39–0.54 (0.46)	NR–NR (NR)	103–289 (179)	[29]
Limestone	0.25–0.47 (0.35)	0.78–0.99 (0.91)	53–151 (103)	[30]
Limestone	0.39–0.43 (0.42)	NR–NR (NR)	47–95 (71)	[31]
Sandstone	0.27–0.43 (0.37)	0.61–0.83 (0.71)	54–167 (96)	The present study

The values were obtained from the referenced papers, adopting directly and recalculating from relevant tables and figures

NR not reported

[a]Average value of relevant variables

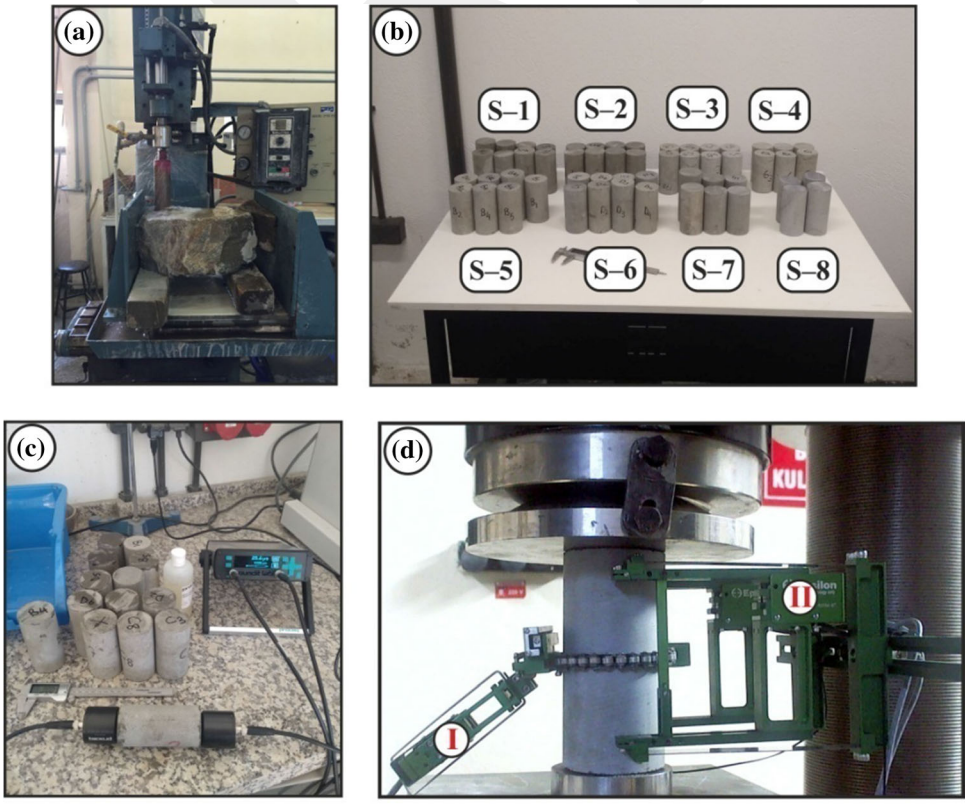

Fig. 2 Laboratory equipment and materials used in laboratory studies. **a** Drilling procedure, **b** some of the cylindrical samples prepared, **c** pulse wave velocity test, **d** determination of UCS, E_{ti}, and v_{ti}

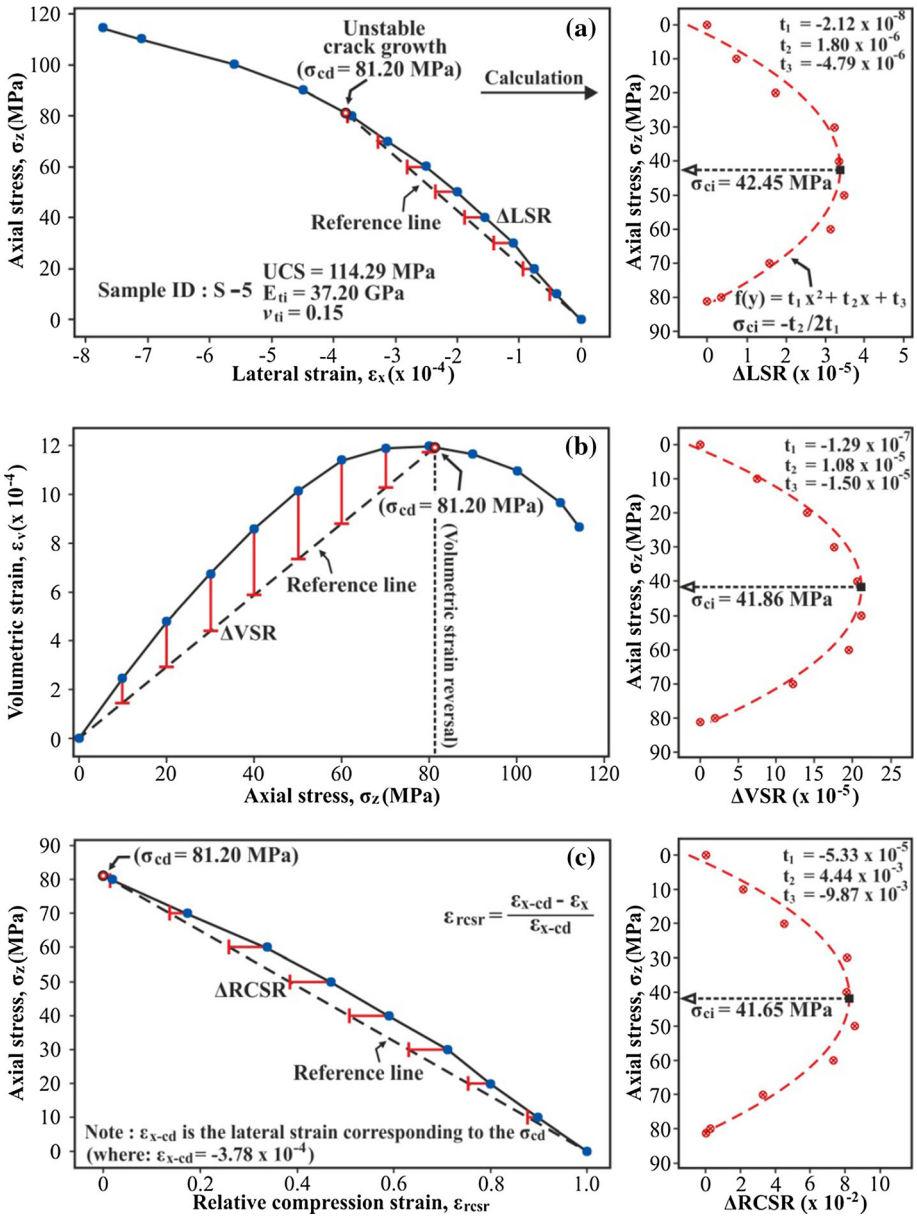

Fig. 3 Quantitative strain-based methods adopted in this study to define the σ_{ci}. **a** LSR method [17], **b** OVS method [18], **c** RCSR method [19]

Fundamental physical and mechanical properties were determined for each rock type. Based on the stress–strain relations of the rocks, the variations in σ_{ci} and σ_{cd} were investigated.

Materials and Methods

Representative rock blocks of the sandstones were obtained from several underground coal mines in the ZHB, and they were used to prepare rock samples for laboratory studies. The determination of physical [i.e., dry unit weight, γ_d (kN/m^3), and effective porosity, n_e (%)], and mechanical properties [UCS (MPa), pulse wave velocity, V_p (km/s), tangential Young modulus, E_{ti} (GPa), and tangential Poisson's ratio, ν_{ti}] was conducted in accordance with the suggestions of International Society of Rock Mechanics [40]. For this purpose, representative rock blocks were drilled using a drill core with a diameter of 54.7 mm (Fig. 2a). Following the drilling procedure, cylindrical core samples were prepared for each rock type (Fig. 2b). The physical and mechanical rock properties were determined, using core samples with a length-to-diameter ratio of 2.0–3.0 under oven-dried conditions.

The pulse wave velocity (V_p, km/s) of the sandstones was determined using a Pundit Plus ultrasonic testing apparatus (Fig. 2c). For each rock sample, ten measurements of pulse waves were recorded and average values were presented. The UCS and static elastic constants (i.e., E_{ti} and ν_{ti}) were determined using a stiff loading machine

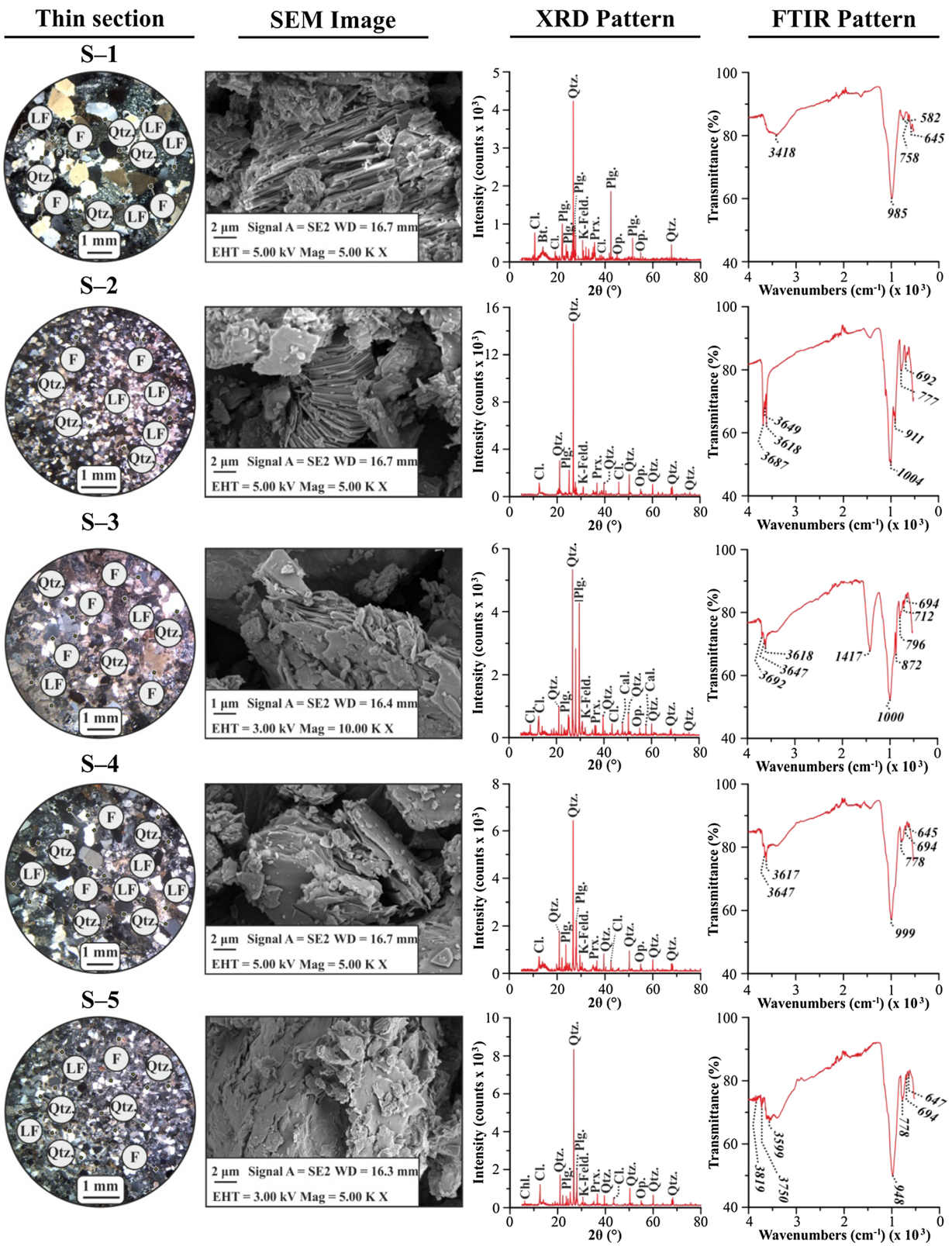

Fig. 4 Typical thin sections, SEM images, XRD, and FTIR patterns of the sandstones [*Qtz* quartz, *Plg* plagioclase, *K-Feld*. alkali feldspar, *Prx* pyroxene, *Bt* biotite, *Cal* calcite, *Chl*. chlorite, *Op* opaque minerals, *Cl*. clay minerals, *F* feldspar (including both Plg and K-Feld. minerals), LF: lithic fragment (including Prx., Bt., Cal., Op., etc.)]

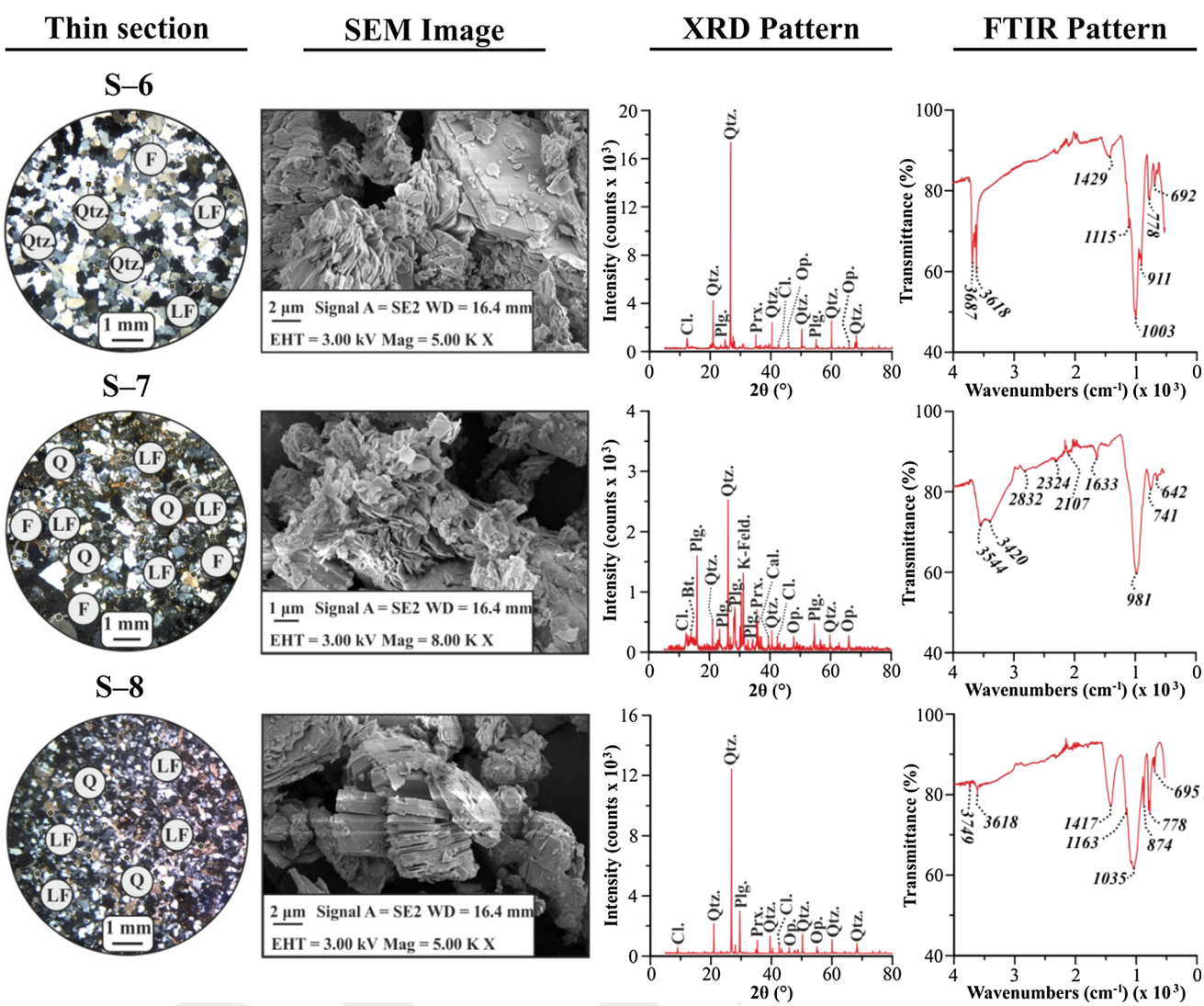

Fig. 4 continued

whose stress rate was within the limits of 0.5–1.0 MPa per second. In order to measure lateral and axial displacements, linear variable differential transformers (LVDT) were utilized (Fig. 2d).

Since previous methods (i.e., Lajtai [1], Brace et al. [13], and Stacey [14]) estimating the σ_{ci} necessitate drawing tangential lines, these methods could be declared somewhat subjective or variable according to users [18, 41]. Therefore, more precise and objective methods to estimate the σ_{ci} were adopted in the present study. These are lateral strain response (LSR) method [17], objective volumetric strain response (OVS) method [18], and relative compression strain (RCSR) method [19].

The implementation and calculation steps of the above-mentioned methods are illustrated in Fig. 3. The implementation of the above-mentioned methods starts with the determination of σ_{cd}. Practically, the σ_{cd} represents the stress state corresponding to the point of ε_v reversal [13]. Establishing a reference line between the zero point (i.e., $\sigma_z = 0$) and the σ_{cd}, the strain differences between the reference line and relevant axial stress–strain curve (e.g., lateral strain difference plotted with red line segments, ΔLSR) were calculated for several axial stress states. The variations in strain differences as independent variables form a parabola [e.g., $f(\sigma_z) = t_1x^2 + t_2x + t_3$], and the peak of this parabola is defined as the σ_{ci} (i.e., $\sigma_{ci} = -t_2/2t_1$). In the light this description, the σ_{ci} was determined using the methods given in Fig. 3.

Mineralogical and textural features of rock materials were investigated through thin sections, X-ray diffraction (XRD), and Fourier transform infrared (FTIR) analyses. In those analyses, quantities of rock-forming minerals and textures properties (i.e., grain size, sorting of grains) were

Table 2 Mineralogical composition of the sandstones

Rock type	Qtz. (%)	Plg. (%)[a]	K-Feld. (%)[b]	LF. (%)[c]	Clay content, C_c (%)[d,e]	Cement type	Classification (according to Folk [42])
S-1	31	26	2	37	4	Silica–clay	Feldspatic litharenite
	29	25	1	36	9		
	34	20	1	40	5		
S-2	57	12	1	25	5	Silica–clay	Feldspatic litharenite
	58	14	1	23	8		
	54	13	2	24	7		
S-3	35	27	1	27	10	Silica–clay–carbonate	Feldspatic litharenite
	36	23	1	32	8		
	34	25	1	35	5		Lithic arkose
S-4	44	13	2	33	8	Silica–clay	Feldspatic litharenite
	48	11	1	35	5		
	46	14	–	35	5		
S-5	52	16	2	22	8	Silica–clay	Feldspatic litharenite
	56	16	1	25	2		
	50	12	2	30	6		Lithic arkose
S-6	78	4	–	16	2	Silica–clay	Sublitharenite
	80	4	–	11	5		
	75	4	–	19	2		
S-7	36	22	5	30	7	Silica–clay	Feldspatic litharenite
	30	16	3	42	9		
	34	18	4	38	6		
S-8	69	11	–	15	5	Silica–clay	Feldspatic litharenite
	72	7	–	17	4		
	77	6	–	11	6		Sublitharenite

[a]Plagioclase (Plg) minerals include albite (Na-rich)–anorthite (Ca-rich) series

[b]Alkali feldspars (K-Feld.) are mainly orthoclase and microcline presenting gridiron twinning

[c]Lithic fragments (LF) comprise: (1) gravel substitutions such as micro-quartzite with undulose extinction and volcano sedimentary particles, (2) detritic igneous constituents (i.e., hornblende, biotite, tremolite, actinolite, annite, chlorite, and pyroxene minerals), (3) carbonate-based fragments (i.e., calcite, aragonite, etc.), (4) opaque minerals (i.e., magnetite, ilmenite, etc.)

[d]clay minerals (i.e., illite, montmorillonite, etc.)

[e]Clay contents were calculated, considering SEM, XRD, and FTIR analysis results

determined. Furthermore, the number of C_c in the sandstones was also investigated through scanning electron microscope (SEM) analyses.

The XRD analyses were carried out, using a Bruker D8 diffractometer, whereas FTIR and SEM analyses were performed through a Thermo Scientific Nicolet 6700 spectrometer and Gemini SEM 300 analyzer, respectively. In addition, textural properties of rock materials were investigated through modal analyses of thin sections.

For each rock sample, four thin sections (two pieces at bottom and upper surfaces) perpendicular to loading direction were prepared. In thin section observations, the point-counting method was adopted to quantify rock-forming minerals. The XRD patterns were analyzed, using Panalytical Highscore Plus software with a database of PDF 2, so that the quantities of rock-forming minerals were determined semiquantitatively.

The FTIR patterns were also utilized to reveal common rock-forming mineral types and possible cement type of the sandstones. Wavenumbers (cm^{-1}) obtained from the FTIR analyses were compared with the XRD patterns, thin section analyses, and relevant previous studies as well. Based on the quantities of rock-forming minerals, the sandstones were classified according to Folk [42].

Texture-based variations in the sandstones were revealed, considering the sorting coefficient (S_c) and average grain size (d_{50}, mm). The determination of the S_c deals with calculating surface areas of rock-forming minerals and analyzing them for specific areas occupied in thin sections. The surface area of any rock-forming mineral is

Table 3 Modal analysis results of the sandstones

Rock type	φ_{95}	φ_{84}	φ_{50}	φ_{16}	φ_5	S_c^a	d_{50} (mm)	n^b	Sorting classification (Folk and Ward [43])[c]
S-1	5.606	4.189	0.765	− 0.192	− 1.959	2.241	0.713	974	Very poorly sorted
	5.240	3.852	0.643	− 0.105	− 1.801	2.056	0.725	810	Very poorly sorted
	5.584	4.481	0.894	− 0.216	− 2.042	2.329	0.689	871	Very poorly sorted
S-2	4.310	3.777	2.963	2.148	1.616	0.815	0.148	1124	Moderately sorted
	4.165	3.842	2.883	2.013	1.491	0.862	0.164	1210	Moderately sorted
	4.152	3.910	3.048	1.881	1.596	0.894	0.129	1058	Moderately sorted
S-3	3.325	2.310	0.766	− 0.111	− 1.412	1.323	0.622	1160	Poorly sorted
	3.683	2.684	0.742	− 0.125	− 1.391	1.471	0.741	1281	Poorly sorted
	3.547	2.273	0.872	− 0.083	− 0.940	1.269	0.595	1314	Poorly sorted
S-4	4.158	3.246	1.513	− 0.125	− 0.489	1.547	0.426	1047	Poorly sorted
	4.450	3.672	1.893	− 0.347	− 0.764	1.795	0.374	956	Poorly sorted
	4.673	3.349	1.438	− 0.095	− 0.559	1.653	0.440	891	Poorly sorted
S-5	5.364	4.692	3.663	2.635	1.962	1.029	0.098	1020	Poorly sorted
	5.725	5.022	3.947	2.873	2.170	1.076	0.083	1322	Poorly sorted
	6.098	5.419	4.379	3.340	2.660	1.040	0.061	1139	Poorly sorted
S-6	3.162	2.635	1.526	0.996	0.460	0.819	0.318	863	Moderately sorted
	3.005	2.410	1.793	0.895	0.524	0.755	0.244	798	Moderately sorted
	3.250	2.468	1.671	0.840	0.482	0.826	0.276	904	Moderately sorted
S-7	5.938	4.492	1.453	0.645	− 0.407	1.923	0.389	1088	Poorly sorted
	6.472	5.502	1.279	0.205	− 0.762	2.345	0.402	1038	Very poorly sorted
	6.094	4.581	1.176	0.485	− 0.203	1.978	0.366	1126	Poorly sorted
S-8	4.542	3.861	3.404	2.696	2.211	0.644	0.116	1209	Moderately well sorted
	4.614	3.963	3.521	2.819	2.022	0.679	0.081	1124	Moderately well sorted
	4.382	3.805	3.686	2.755	1.998	0.624	0.062	1177	Moderately well sorted

[a]The S_c was determined using Eq. 4

[b]Number of observations in modal analyses

[c]Sorting classification is based on S_c values

digitized using MATLAB R2019a and determined by the following equation:

$$A = \frac{1}{2}\left|\sum_{i=1}^{n} x_i(y_{i+1}) - \sum_{i=1}^{n} y_i(x_{i+1})\right| \quad (1)$$

where x_i and y_i are digitized coordinates of the boundary surfaces.

For specific areas in each thin section (e.g., 30–45 mm^2), surface areas of rock-forming minerals were determined and analyzed statistically. Based on the assumption that the anhedral grains could be acknowledged somewhat spherical or elliptical for sandstones, the surface area determined by Eq. 1 was equalized to the area of a circle in two dimensions.

Consequently, the S_c is determined by the following equations:

$$D_e = \sqrt{\frac{4A}{\pi}} \quad (2)$$

where D_e is the equivalent diameter of the grain (mm) and A is the surface area of the grain (mm^2) determined by Eq. 1.

$$\varphi = -\log_2(D_e) \quad (3)$$

where φ is the size value of the grain; D_e is in mm.

$$S_c = \frac{\varphi_{84} - \varphi_{16}}{4.0} + \frac{\varphi_{95} - \varphi_5}{6.6} \quad (4)$$

where φ_{95}, φ_{84}, φ_{16}, and φ_5 represent the size values at 95%, 84%, 16%, and 5% at cumulative percentages, respectively [43].

Table 4 Physical and mechanical properties of the sandstones

Rock type	γ_d (kN/m^3)	n_e (%)	V_p (km/s)	E_{ti} (GPa)	ν_{ti}	$\sigma_{ci(LSR)}$ (MPa)	$\sigma_{ci(OVS)}$ (MPa)	$\sigma_{ci(RCSR)}$ (MPa)	$\sigma_{ci(mean)}$ (MPa)	σ_{cd} (MPa)	UCS (MPa)	$\sigma_{ci(mean)}$/ UCS	σ_{cd}/ UCS
S-1	23.82	5.43	2.71	16.01	0.24	23.50	22.35	24.23	23.36	50.12	79.41	0.29	0.63
	23.87	5.20	2.94	20.58	0.22	21.14	19.70	20.44	20.43	48.87	75.30	0.27	0.65
	23.68	7.86	2.52	10.52	0.25	20.99	18.76	21.30	20.35	44.51	66.53	0.31	0.67
S-2	25.20	1.80	3.98	24.74	0.21	40.38	38.62	41.09	40.03	70.96	95.56	0.42	0.74
	24.93	1.72	4.05	25.40	0.21	38.90	37.52	37.30	37.91	68.06	92.17	0.41	0.74
	24.77	2.09	3.22	21.39	0.20	36.67	35.18	37.01	36.29	62.25	87.44	0.41	0.71
S-3	23.80	3.50	2.75	13.26	0.27	24.64	23.05	25.48	24.39	48.54	69.09	0.35	0.70
	23.85	3.94	2.58	15.13	0.25	22.05	19.44	21.95	21.15	40.70	60.27	0.35	0.68
	24.25	4.23	2.54	13.27	0.24	21.80	20.66	22.14	21.53	39.61	58.74	0.37	0.67
S-4	23.64	5.94	2.88	17.19	0.23	24.04	21.62	23.35	23.00	45.68	63.47	0.36	0.72
	23.84	6.08	2.99	12.09	0.28	20.09	20.43	21.27	20.60	37.31	54.19	0.38	0.69
	24.02	6.47	2.65	14.80	0.25	22.56	18.75	20.93	20.75	41.29	59.28	0.35	0.70
S-5	24.82	1.25	4.43	37.20	0.15	42.45	41.86	41.65	41.99	81.20	114.29	0.37	0.71
	25.10	0.94	4.27	32.20	0.12	43.62	42.19	43.05	42.95	79.81	106.54	0.40	0.75
	24.92	1.30	4.51	35.86	0.14	40.28	39.56	41.30	40.38	76.11	102.26	0.39	0.74
S-6	26.31	1.95	4.15	25.32	0.25	47.50	42.83	46.90	45.74	89.84	115.09	0.40	0.78
	26.63	1.87	4.22	32.77	0.22	56.75	55.62	55.99	56.12	117.35	140.58	0.40	0.83
	26.07	1.68	3.90	29.92	0.26	52.37	53.02	53.26	52.88	95.64	124.16	0.43	0.77
S-7	25.21	2.37	3.66	24.31	0.24	33.54	31.06	33.62	32.74	65.10	106.73	0.31	0.61
	25.42	1.00	3.52	21.15	0.23	31.85	30.60	32.28	31.58	62.23	97.46	0.32	0.64
	25.34	1.46	3.50	18.57	0.24	32.43	29.61	31.60	31.21	64.16	92.25	0.34	0.70
S-8	26.65	0.79	4.33	25.35	0.16	53.08	51.37	52.75	52.40	100.25	139.16	0.38	0.72
	26.38	0.86	4.51	29.11	0.15	52.19	51.77	52.44	52.13	102.70	149.74	0.35	0.69
	26.24	0.92	4.62	29.61	0.15	66.40	63.61	64.22	64.74	121.05	166.57	0.39	0.73

γ_d dry unit weight, n_e effective porosity, V_p pulse wave velocity, E_t tangential Young modulus, ν_{ti} tangential Poisson's ratio, $\sigma_{ci(LSR)}$ crack initiation stress obtained through the LSR method, $\sigma_{ci(OVS)}$ crack initiation stress obtained through the OVS method, $\sigma_{ci(RCSR)}$ crack initiation stress through the RCSR method, $\sigma_{ci(mean)}$ average crack initiation stress of three strain-based methods, σ_{cd} crack damage stress

Laboratory Studies

Mineralogical and Textural Properties

Typical thin sections, SEM images showing the presence of clay content, XRD, and FTIR patterns of the sandstones are given in Fig. 4. From mineralogical and textural points of view, it is obvious that the sandstones differ from one another. Based on the mineralogical inspections, mineralogical compositions of the sandstones are given in Table 2.

According to the classification of Folk [42], the sandstones were identified, varying from Sublitharenite to Lithic arkose. The cement type of the sandstone mainly comprises the mixture of silica and clay particles lower than 20 μm.

Focusing on the SEM and FTIR analyses, it was determined that the C_c in the sandstones differs at average rates of 2–10%. The types of clay particles are mainly illite, montmorillonite, and sometimes kaolinite.

In the FTIR patterns, clay particles are typically characterized with wavenumbers between 3418 and 3819 cm^{-1}, whereas siliceous minerals (quartz, feldspar, etc.) are characterized by wavenumbers ranged from 582 to 1163 cm^{-1}. Calcium-based mineral associations (i.e., calcite, aragonite, Ca–rich plagioclases) are observed at wavenumbers between 1417 and 2832 cm^{-1}.

The modal analysis results are given in Table 3. The d_{50} of the sandstones was found to be between 0.061 and 0.741 mm. Based on the S_c classification of Folk and Ward [43], the sandstones were identified as from moderately well to very poorly sorted. Furthermore, during modal analyses, it was determined that the increase in LF contents results in achieving higher S_c values. However, combining the values given in Tables 2 and 3, it could be claimed that there is no remarkable relationship between the S_c and C_c.

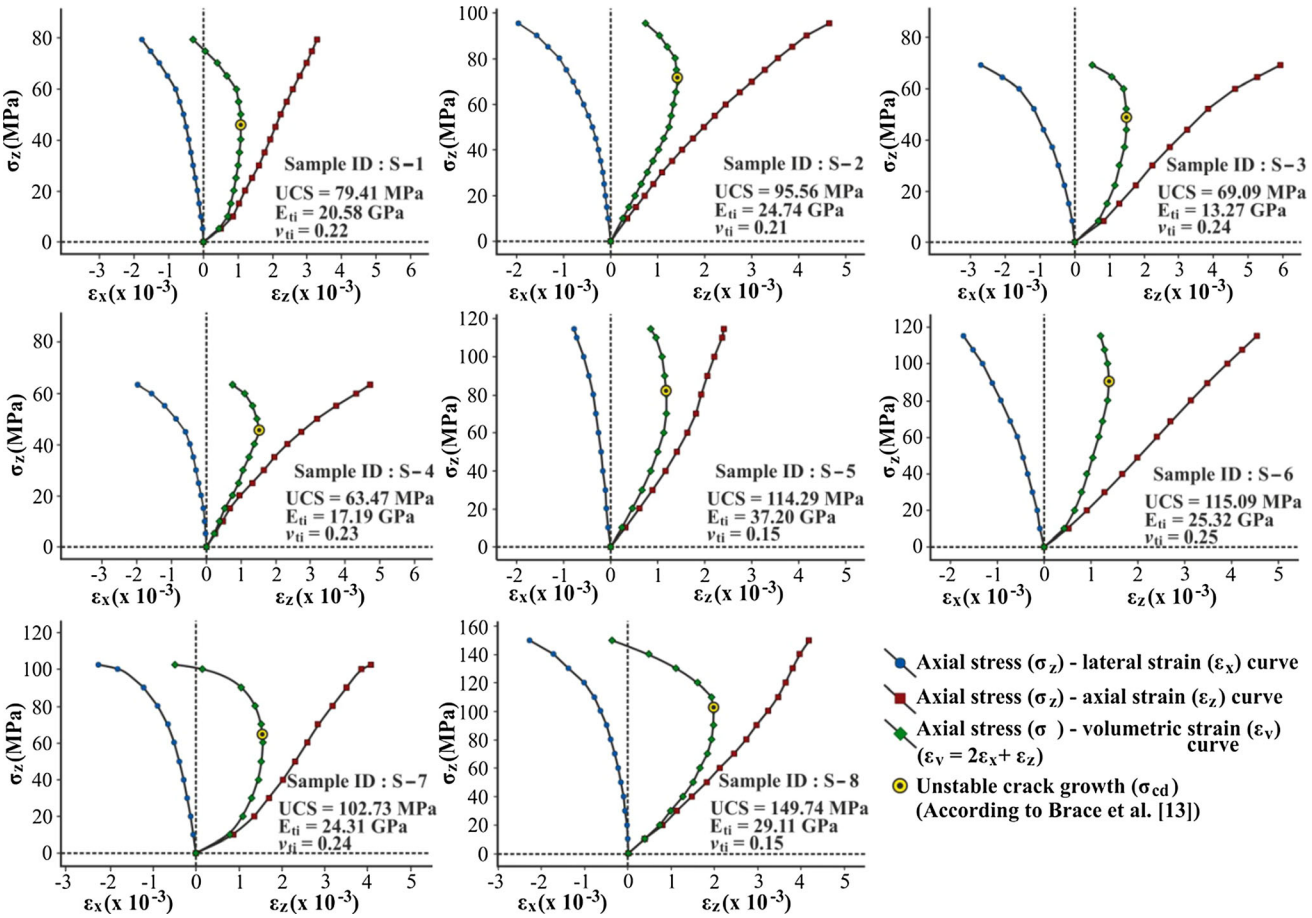

Fig. 5 Typical stress–strain curves of the sandstones

Table 5 Pearson's correlation matrix of the mineralogical and textural features

Parameter	S_c	d_{50}	Qtz.	F	LF	C_c
$\sigma_{ci(mean)}$	− 0.776	− 0.793	0.884	− 0.756	− 0.888	− 0.365
σ_{cd}	− 0.710	− 0.724	0.854	− 0.729	− 0.871	− 0.340
$\sigma_{cd}/\sigma_{ci(mean)}$	0.594	0.602	− 0.400	0.380	0.347	0.200
$\sigma_{ci(mean)}$/UCS	− 0.825	− 0.704	0.748	− 0.702	− 0.651	− 0.375
σ_{cd}/UCS	− 0.745	− 0.560	0.793	− 0.772	− 0.707	− 0.361

S_c sorting coefficient, d_{50} average grain size (mm), *Qtz* quartz content (%), *F* Feldspar content (%) is the sum of Plg. and K-Feld. minerals, *LF* lithic fragment content (%), C_c clay content (%)

Physical and Mechanical Properties

The physical and mechanical properties of the sandstones are listed in Table 4. It was determined that the UCS of the sandstones is between 54 and 167 MPa. The n_e is approximately between 0.8 and 8.0%. The V_p of the sandstones varies from 2.50 to 4.60 km/s. The static elastic constants of E_{ti} and ν_{ti} vary also between 10–38 GPa and 0.12–0.28, respectively. Typical stress–strain curves of the sandstones are given in Fig. 5.

Using these stress–strain curves of the sandstones, the σ_{ci} and σ_{cd} were determined according to the methods mentioned previously in "Materials and Methods" section. As a result, the σ_{ci} and σ_{cd} were found to be in the range of 0.27–0.43 and 0.61–0.83 of the UCS, respectively. In general, it was determined that the σ_{ci} and σ_{cd} correspond to 0.37 and 0.71 of the UCS, respectively.

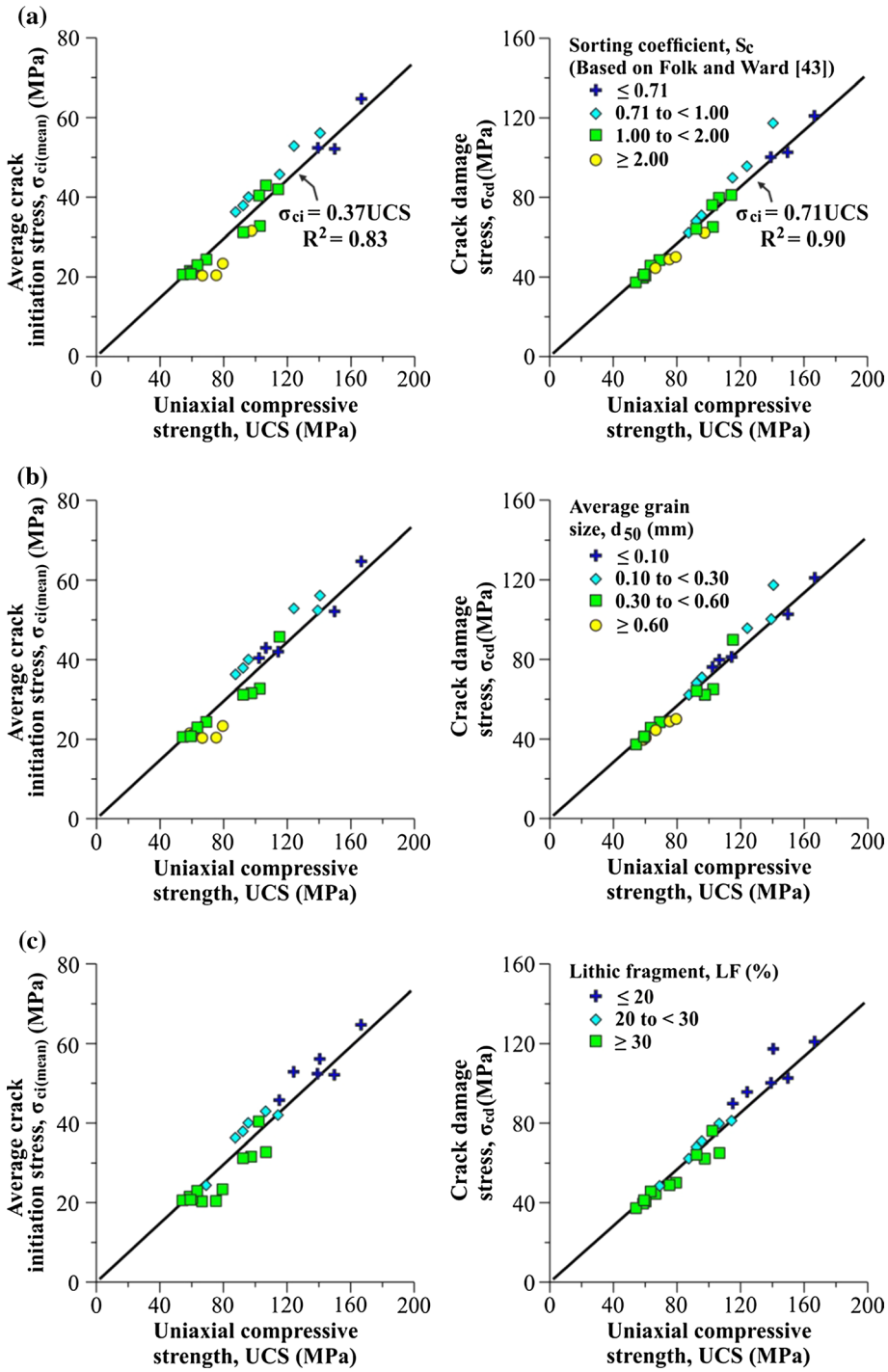

Fig. 6 Variations in σ_{ci} and σ_{cd} due to several mineralogical and textural features. **a** The S_c, **b** the d_{50}, **c** the content of LF

Results and Discussion

Effects of Mineralogical and Textural Features on the σ_{ci} and σ_{cd}

It was determined that the fracture evolution of the sandstones is associated with the variations in mineralogical and textural features. For instance, the σ_{ci} and σ_{cd} decrease with increasing the d_{50}, S_c, and contents of F and LF, whereas they increase in parallel with Qtz content. The effects of mineralogical and textural features on the strength properties are summarized in Table 5.

It can also be seen in Table 5 that the ratio of $\sigma_{cd}/\sigma_{ci(mean)}$ increases with increasing the S_c and d_{50}. Since

Table 6 Pearson's correlation matrix of the physico-mechanical properties

Parameter	γ_d	n_e	UCS	V_p	E_{ti}	ν_{ti}
$\sigma_{ci(mean)}$	0.915	− 0.791	0.961	0.901	0.812	− 0.602
σ_{cd}	0.922	− 0.753	0.978	0.885	0.806	− 0.583
$\sigma_{cd}/\sigma_{ci(mean)}$	− 0.245	0.438	–	− 0.322	− 0.233	0.201
$\sigma_{ci(mean)}$/UCS	0.474	− 0.497	–	0.527	0.473	− 0.263
σ_{cd}/UCS	0.531	− 0.394	–	0.546	0.539	− 0.243

γ_d dry unit weight (kN/m^3), n_e effective porosity (%), *UCS* uniaxial compressive strength (MPa), V_p pulse wave velocity (km/s), E_{ti} tangential Young Modulus (GPa), ν_{ti} tangential Poisson's ratio

the higher values of S_c describe heterogeneity in the rock itself, the σ_{ci} and σ_{cd} decrease with increasing the S_c (Fig. 6a). Increasing d_{50} also acts on the σ_{ci} and σ_{cd} in a similar manner to that of the S_c (Fig. 6b). From mineralogical perspectives, the increase in the content of LF also poses heterogeneity in the rocks and therefore reduces the strength properties (Fig. 6c).

The decrease in σ_{ci} and σ_{cd} arising from textural and physico-mechanical properties might be interpreted, referring to release surfaces enlarged exponentially in the rock itself and therefore dislocation of grains during axial loading. As given in Fig. 6, though the interrelation between the S_c and d_{50} is not obvious, their variations together could provide satisfactory results in assessing the heterogeneity in the sandstones. The adverse effects of increase in grain size on strength properties of various rock types were also reported by several researchers [3, 25, 33, 34, 44–46]. From this aspect, the findings given in Fig. 6 are in good agreement with these studies.

Effects of Physico-Mechanical Features on the σ_{ci} and σ_{cd}

Laboratory studies showed that the σ_{ci} and σ_{cd} increase with decreasing n_e, whereas they increase with increasing the properties of γ_d, UCS, V_p, and E_{ti} (Table 6). In particular, the first cracks in the rock itself were initiated much earlier when the n_e of rocks exceeds 3% (Fig. 7a). When it comes to the changes in V_p values, remarkable changes in the σ_{ci} and σ_{cd} were obtained when the V_p exceeds 3.00 km/s (Fig. 7b). In the direction of these findings, apart from the UCS, it could be claimed that fracture evolution of the sandstones could also be assessed, considering the variations in n_e and V_p values.

Moreover, it was also revealed that the crack initiation and propagation in the sandstones are independent from the Modulus ratio (MR: E_{ti}/UCS). However, the fracture evolution of the sandstones seems to be associated with the static elastic constants of E_{ti} and ν_{ti} (Table 6). The remarkable changes in σ_{ci} and σ_{cd} corresponding to the conditions of $n_e \geq 3\%$ and $V_p \geq 3.00$ km/s could be declared the threshold values that might pave the way for estimations relating strata control and stability analyses of the longwalls and galleries whose roof strata of longwalls located in the ZHB are composed of the investigated sandstones.

Statistical Analyses

Based on the mineralogical analyses and laboratory test results (Tables 2, 3, 4), statistical analyses were performed. Excluding the UCS as an independent variable, statistically remarkable relationships are listed in Table 7. In general, the statistical analyses indicated that textural features of sandstones could take a part in the assessment of crack initiation for the sandstones.

In view of the fact that the correlation of determinations (R^2) for Eqs. 2 and 3 (0.58 and 0.61, respectively) is greater than those of Eqs. 10 and 11 (0.48 and 0.50, respectively), it is clear that the textural features of d_{50} and S_c are relatively more influential in estimating the σ_{ci} rather than the σ_{cd}. Similar results could also be observed, comparing the R^2 of Eq. 14 (0.67) with that of Eq. 15 (0.53). In the light of this finding, it is possible to state that the textural features are reasonable factors that affect crack initiation of the sandstones investigated.

In terms of mineralogical effects on fracture evolution of the sandstones, the increase in the LF content gives rise to pose heterogeneity that has similarities with the effects of S_c. Therefore, its increase lowers the σ_{ci} and σ_{cd} (Eqs. 1 and 9 in Table 7). As for the mineralogical and physico-mechanical features, the σ_{ci} could be predicted reliably, using Eqs. of 1 and 5–8. However, other relationships such as Eqs. 9 and 13 could be utilized to predict the σ_{cd} (Table 7).

According to the strain-based methods to quantify the σ_{ci}, it was statistically determined that the OVS method provides σ_{ci} values approximately 4% lower than those of

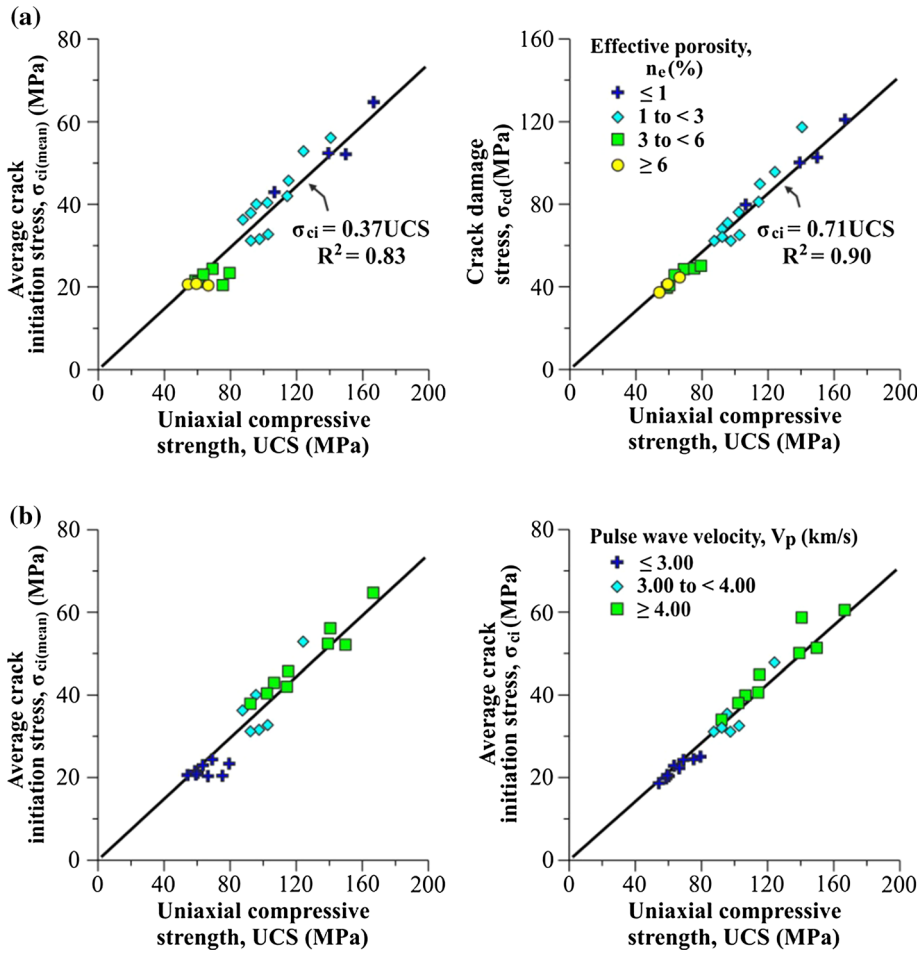

Fig. 7 Variations in σ_{ci} and σ_{cd} due to several physical and mechanical properties. **a** The n_e, **b** the V_p

the LSR and RCSR methods (Eqs. 17, 18). On the other hand, the methods of LSR and RCSR methods provide nearly similar results (Eq. 18).

Links to Utilization of Mineralogical and Textural Features for Underground Excavations in the ZHB

In the direction of the previous studies [3–7], it seems logical to suppose that crack initiation could be explored for *V*-cut gallery blasting operations and overburden analyses in the ZHB. In this respect, the findings obtained from the present study could contribute to those of applications.

According to practices on *V*-cut gallery blasting operations in the ZHB, it could be acknowledged that mineralogical and textural analyses in the direction of sandstone lithofacies for underground coal mining are not taken into consideration. However, focusing on systematical records of mineralogical and textural features, practical experiences and data could be collected for relevant engineers in the ZHB. With the help of these systematical records through sampling/logging, an example of which is illustrated in Fig. 8, the optimization of explosive consumption in a gallery blasting could be explored.

In Fig. 8, a gallery face, which is composed of a single sandstone stratum and observed frequently in the ZHB, is given as Case I. For single but various sandstone lithofacies, crack initiation stress thresholds in conjunction with rock mass classifications [47, 48] could be a key parameter for the optimization of gallery blasting operations and overburden control. Within this scope, present and upcoming gallery faces should be explored profoundly from mineralogical and textural perspectives. It may cover several stages including a dataset, where the amount of explosive consumption and its blasting pattern per *V*-cut operation, the quantitative data intentionally blanked for other sandstone lithofacies in Fig. 8, amount of face advance after blasting and overburden observations might be present. Thanks to this comprehensive dataset, sensitive analysis could be carried out for the optimization of *V*-cut gallery blasting operations.

On the other hand, considering the presence of lithological changes followed by face advance (e.g., the

Table 7 Statistical analysis results

Independent variable	Equations	No.	Estimate	SE	*t* value	*F* value	R^2
LF	$\sigma_{ci(mean)} = 71.07 - 1.29LF$	1	71.07	4.13	17.21	81.92	0.77
			− 1.29	0.14	− 9.21		
S_c	$\sigma_{ci(mean)} = 59.68 - 18.05S_c$	2	59.68	4.52	13.19	33.40	0.58
			− 18.05	3.12	− 5.78		
d_{50}	$\sigma_{ci(mean)} = 51.28 - 45.51d_{50}$	3	51.28	3.09	16.61	37.19	0.61
			− 45.51	7.46	− 6.10		
n_e	$\sigma_{ci(mean)} = 50.21 - 4.96n_e$	4	50.21	2.96	16.96	36.70	0.60
			− 4.96	0.82	6.05		
V_p	$\sigma_{ci(mean)} = -22.46 + 16.32V_p$	5	− 22.46	6.09	− 3.69	94.64	0.80
			16.32	1.68	9.73		
Qtz., V_p	$\sigma_{ci(mean)} = -18.56 + 0.37Qtz + 9.89V_p$	6	− 18.56	4.37	4.25	107.12	0.90
			0.37	0.08	4.63		
			9.89	1.78	5.56		
LF, n_e	$\sigma_{ci(mean)} = 68.60 - 0.94LF - 2.44n_e$	7	68.60	3.22	21.30	78.18	0.87
			− 0.94	0.14	6.71		
			− 2.44	0.60	− 4.07		
F^a, n_e	$\sigma_{ci(mean)} = 60.96 - 0.90F - 3.65n_e$	8	60.96	2.62	23.27	63.03	0.84
			− 0.90	0.15	− 6.00		
			− 3.65	0.56	− 6.52		
LF	$\sigma_{cd} = 133.84 - 2.37LF$	9	133.84	8.23	16.27	69.10	0.75
			− 2.37	0.28	− 8.46		
S_c	$\sigma_{cd} = 110.01 - 30.84S_c$	10	110.01	9.44	11.65	22.42	0.48
			− 30.84	6.51	− 4.74		
d_{50}	$\sigma_{cd} = 95.62 - 77.60d_{50}$	11	95.62	6.52	14.67	24.26	0.50
			− 77.60	15.82	− 4.91		
n_e	$\sigma_{cd} = 94.83 - 8.81n_e$	12	94.83	5.94	15.95	28.74	0.54
			− 8.81	1.64	− 5.36		
V_p	$\sigma_{cd} = -37.60 + 29.93V_p$	13	− 37.60	12.24	− 3.07	79.47	0.77
			29.93	3.36	8.91		
S_c	$\sigma_{ci(mean)}/UCS = 0.445 - 0.060S_c$	14	0.445	0.013	34.23	46.91	0.67
			− 0.060	0.009	− 6.67		
S_c	$\sigma_{cd}/UCS = 0.793 - 0.064S_c$	15	0.793	0.018	44.06	27.40	0.53
			− 0.064	0.012	− 5.34		
$\sigma_{ci(LSR)}$	$\sigma_{ci(OVS)} = 0.960\sigma_{ci(LSR)}$	16	0.960	0.0070	137.14	–	0.93
$\sigma_{ci(RCSR)}$	$\sigma_{ci(OVS)} = 0.966\sigma_{ci(RCSR)}$	17	0.966	0.0068	142.06	–	0.93
$\sigma_{ci(LSR)}$	$\sigma_{ci(RCSR)} = 0.994\sigma_{ci(LSR)}$	18	0.994	0.0047	211.49	–	0.95

Qtz quartz content (%), *LF* lithic fragment content (%), *F* feldspar content ([a]The sum of Plg. and K-Feld. minerals, %), S_c sorting coefficient, d_{50} average grain size (mm), n_e effective porosity (%), V_p pulse wave velocity (km/s), *UCS* uniaxial compressive strength (MPa), $\sigma_{ci(LSR)}$ crack initiation stress through the LSR method (MPa), $\sigma_{ci(OVS)}$ crack initiation stress through the OVS method (MPa), $\sigma_{ci(RCSR)}$ crack initiation stress through the RCSR method (MPa), $\sigma_{ci(mean)}$ average crack initiation stress (MPa), σ_{cd} crack damage stress (MPa)

transition between Case I and Case II in Fig. 8), stability analyses in conjunction with rock mass fracturing beyond the acceptable excavation line and over breaking minimization in gallery blasting operations could also be performed. In this context, stability considerations given by Gerçek [49] could be highly appreciated. Last but not least, hydraulic fracturing applications could be enhanced or

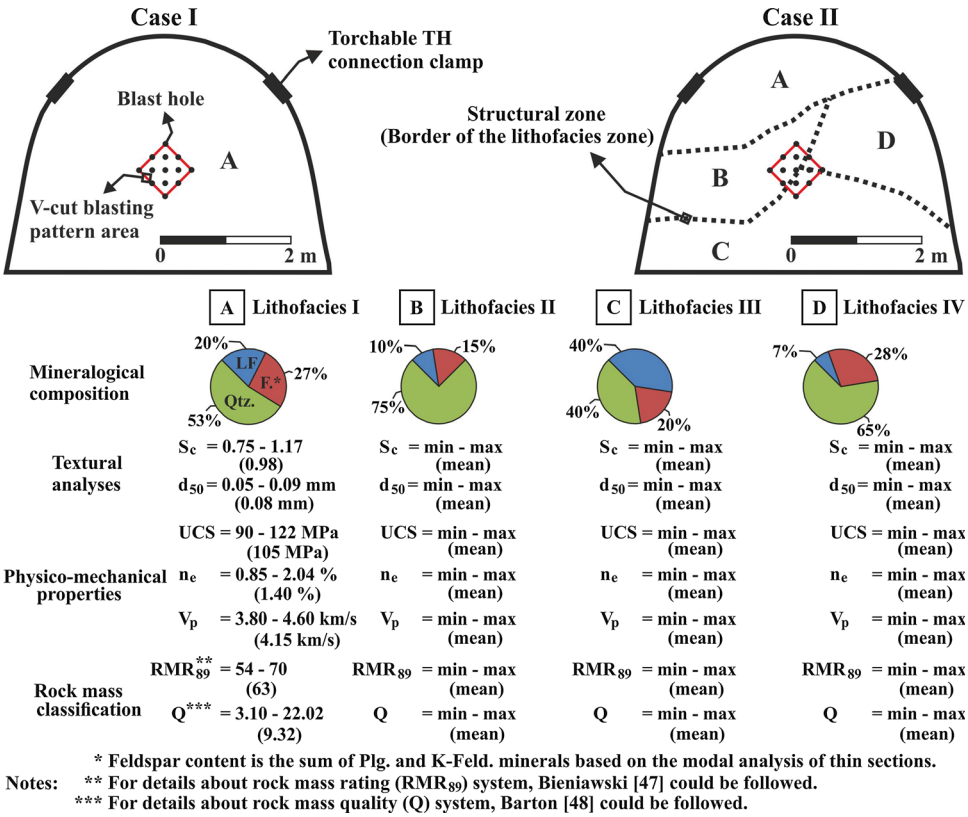

Notes: * Feldspar content is the sum of Plg. and K-Feld. minerals based on the modal analysis of thin sections.
** For details about rock mass rating (RMR_{89}) system, Bieniawski [47] could be followed.
*** For details about rock mass quality (Q) system, Barton [48] could be followed.

Fig. 8 Simplified illustration of systematical data recording for the assessment of *V*-cut gallery blasting optimization

further investigated, considering rock mineralogy and texture for various sandstone facies.

Conclusions

The present study investigates the factors affecting the fracture evolution of the sandstones located in the ZHB. For this purpose, detailed mineralogical and textural analyses were performed on eight coal measure sandstones. Physico-mechanical properties of the rocks were determined. The σ_{ci} and σ_{cd} were determined for each rock type, considering quantitative strain-based methods. The laboratory studies indicate that mineralogical, textural, and physico-mechanical features have substantial effects on the σ_{ci} and σ_{cd}. The other results obtained from the present study could be drawn as follows:

- The σ_{ci} and σ_{cd} are found to be at average rates of 0.37 and 0.71 of the UCS, respectively (Table 4). The σ_{ci} and σ_{cd} decrease with increasing the S_c, d_{50}, F, LF of the rocks. On the other hand, increasing Qtz content leads to increase those variables (Table 5). Remarkable changes are determined in those variables when the n_e and V_p exceed 3% and 3.00 km/s, respectively (Fig. 7).
- When comparing the strain-based methods to quantify the σ_{ci}, it was determined that the OVS method provides σ_{ci} values approximately 4% lower than those of the LSR and RCSR methods do. The methods of LSR and RCSR methods provide more or less similar results (Table 7).
- With the purpose of utilizing the mineralogical and textural features in underground mining applications in the ZHB, several suggestions related to *V*-cut gallery blasting operations were given. Considering the achievements obtained from the present study, *V*-cut gallery blasting operations could be optimized. Thus, the amount of explosive consumption during *V*-cut operations and overburden problems could be handled elaborately. However, *V*-cut blasting applications/case studies are required to examine whether rock texture and mineralogy would be effective as much as the laboratory test results obtained.
- It should be mentioned that the laboratory studies were performed under oven-dried conditions. Considering the saturation degree of the rock materials, fracture evolution of rocks should also be investigated by further studies. By this way, the relationship between mineralogy and dehydration of rocks could be explored in terms of fracture mechanics.

- Since underground coal mining applications in the ZHB are gradually carried out at greater depths, the fracture evolution of the rocks should be investigated by triaxial compression tests.

Acknowledgements The author is greatly indebted to staff members; Birol KARAÇAM and Dinçer ACUN (Mining engineers), Mehmet KUZU and Miraç KOCA (Topographers), Turan ZARARCI, Aydın EKİNCİ, Erhan KEÇELİOĞLU and Şendoğan ÖZAT (Mining technicians) of Turkish Hard Coal Enterprise Institution (TTK, Zonguldak—Turkey) for their invaluable help at obtaining rock blocks and sharing experiences during underground field observations. The author also appreciates the constructive comments and suggestions of the editor and anonymous reviewers.

References

1. Lajtai EZ (1974) Brittle fracture in compression. Int J Fract Mech 10:525–536. https://doi.org/10.1007/BF00155255
2. Eberhardt E, Stead D, Stimpson B, Read R (1998) Identifying crack initiation and propagation thresholds in brittle rocks. Can Geotech J 35(2):222–233. https://doi.org/10.1139/t97-091
3. Cai M, Kaiser PK, Tasaka Y, Maejima T, Morioka H, Minami M (2004) Generalized crack initiation and crack damage stress thresholds of brittle rock masses near underground excavations. Int J Rock Mech Min Sci 41:833–847. https://doi.org/10.1016/j.ijrmms.2004.02.001
4. Diederichs M, Kaiser P, Eberhardt E (2004) Damage initiation and propagation in hard rock during tunnelling and the influence of near-face stress rotation. Int J Rock Mech Min Sci 41(5):785–812. https://doi.org/10.1016/j.ijrmms.2004.02.003
5. Andersson JC, Martin CD, Stille H (2009) The Äspö Pillar stability experiment: part II—rock mass response to coupled excavation-induced and thermal-induced stresses. Int J Rock Mech Min Sci 46:879–895. https://doi.org/10.1016/j.ijrmms.2009.03.002
6. Perras MA, Diederichs MS (2016) Predicting excavation damage zone depths in brittle rocks. Rock Mech Geotech Eng 8(1):60–74. https://doi.org/10.1016/j.jrmge.2015.11.004
7. Martin CD, Christiansson R (2009) Estimating the potential for spalling around a deep nuclear waste repository in crystalline rock. Int J Rock Mech Min Sci 46(2):219–228. https://doi.org/10.1016/j.ijrmms.2008.03.001
8. Damjanac B, Fairhurst C (2010) Evidence for a long-term strength threshold in crystalline rock. Rock Mech Rock Eng 43:513–531. https://doi.org/10.1007/s00603-010-0090-9
9. Jiang H, Du C, Liu S, Gao K (2014) Numerical simulation of rock fragmentation under the impact load of water jet. Shock Vib. https://doi.org/10.1155/2014/219489
10. Lu Y, Zuo S, Ge Z, Xiao S, Cheng Y (2016) Experimental study of crack Initiation and extension induced by hydraulic fracturing in a tree-type borehole array. Energies 9(7):514. https://doi.org/10.3390/en9070514
11. Liu Q, Liu J, Pan Y, Kong X, Hong K (2017) A case study of TBM performance prediction using a Chinese rock mass classification system—hydropower classification (HC) method. Tunnel Underg Space Technol 65:140–154. https://doi.org/10.1016/j.tust.2017.03.002
12. Niu Y, Zhou XP, Zhang JZ, Qian QH (2019) Experimental study on crack coalescence behavior of double unparallel fissure-contained sandstone specimens subjected to freeze-thaw cycles under uniaxial compression. Cold Reg Sci Technol 158:166–181. https://doi.org/10.1016/j.coldregions.2018.11.015
13. Brace WF, Paulding B, Scholz C (1966) Dilatancy in the fracture of crystalline rocks. J Geophys Res 71:3939–3953. https://doi.org/10.1029/JZ071i016p03939
14. Stacey TR (1981) A simple extension strain criterion for fracture of brittle rock. Int J Rock Mech Min Sci Geomech Abstr 18(6):469–474. https://doi.org/10.1016/0148-9062(81)90511-8
15. Martin CD, Chandler NA (1994) The progressive fracture of Lac du Bonnet granite. Int J Rock Mech Min Sci Geomech Abstr 31(6):643–659. https://doi.org/10.1016/0148-9062(94)90005-1
16. Diederichs MS (2007) The 2003 Canadian Geotechnical Colloquium: mechanistic interpretation and practical application of damage and spalling prediction criteria for deep tunnelling. Can Geotech J 44(9):1082–1116. https://doi.org/10.1139/T07-033
17. Nicksiar M, Martin CD (2012) Evaluation of methods for determining crack initiation in compression tests on low-porosity rocks. Rock Mech Rock Eng 45:607–617. https://doi.org/10.1007/s00603-012-0221-6
18. Pengfei L, Jianzhao H, Qingchi C (2014) A volumetric strain-based method to determined crack initiation stress of low-porosity rocks. In: 5th international conference on intelligent systems design and engineering applications 2014, pp 106–108. https://doi.org/10.1109/ISDEA.2014.31
19. Wen T, Tang H, Ma J, Wang Y (2018) Evaluation of methods for determining crack initiation stress under compression. Eng Geol 235:81–97. https://doi.org/10.1016/j.enggeo.2018.01.018
20. Zhao XG, Cai M, Wang J, Li PF, Ma LK (2015) Objective determination of crack initiation stress of brittle rocks under compression using AE measurement. Rock Mech Rock Eng 48:2473–2484. https://doi.org/10.1007/s00603-014-0703-9
21. Yang SQ, Tian WL, Huang YH, Ma GZ, Fan LF, Wu ZJ (2018) Experimental and discrete element modeling on cracking behavior of sandstone containing a single oval flaw under uniaxial compression. Eng Fract Mech 194:154–174. https://doi.org/10.1016/j.engfracmech.2018.03.003
22. Wu H, Zhao G, Liang W (2019) Investigation of cracking behavior and mechanism of sandstone specimens with a hole under compression. Int J Mech Sci 163:105084. https://doi.org/10.1016/j.ijmecsci.2019.105084
23. Lou Y, Zhang G, Wang X (2019) Cracking mode analysis of crack initiation in rocks under uniaxial compression. Adv Civ Eng. https://doi.org/10.1155/2019/5818071
24. Erişiş S, Tuğrul A, Yılmaz Ö, Er S (2019) Investigation of the effects of mineralogic and petrographical characteristics of basaltic rocks on acoustic emission. J Geol Eng 43:1–22. https://doi.org/10.24232/jmd.572450
25. Nicksiar M, Martin CD (2013) Crack initiation stress in low porosity crystalline and sedimentary rocks. Eng Geol 154:64–76. https://doi.org/10.1016/j.enggeo.2012.12.007
26. Zhao XG, Cai M, Wang J, Ma LK (2013) Damage stress and acoustic emission characteristics of the Beishan granite. Int J Rock Mech Min Sci 64:258–269. https://doi.org/10.1016/j.ijrmms.2013.09.003
27. Basu A, Mishra DA (2014) A method for estimating crack initiation stress of rock materials by porosity. J Geol Soc India 84:397–405. https://doi.org/10.1007/s12594-014-0145-8
28. Kim JS, Lee KS, Cho WJ, Choi HJ, Cho GC (2015) A comparative evaluation of stress–strain and acoustic emission methods for quantitative damage assessments of brittle rock. Rock Mech Rock Eng 48:495–508. https://doi.org/10.1007/s00603-014-0590-0
29. Ündül Ö, Amann F, Aysal N, Plötze M (2015) Micro-textural effects on crack initiation and crack propagation of andesitic rocks. Eng Geol 193:267–275. https://doi.org/10.1016/j.enggeo.2015.04.024

30. Ündül Ö, Aysal N, Çobanoğlı BC, Amann F, Perras M (2016) Strength, deformation and cracking characteristics of limestones. In: Ulusay R et al (eds) Rock mechanics and rock engineering: from the past to the future, Nevşehir, Turkey, pp 181–185
31. Köken E (2019) On the variation in several rock properties due to magnesium sulfate weathering tests—a case study for limestones. In: 19th ınternational multidisciplinary scientific geoconference (SGEM 2019), vol 1–2, pp 405–412. https://doi.org/10.5593/2sgem019/1.2/S02.052
32. Nicksiar M, Martin CD (2014) Factors affecting crack initiation in low porosity crystalline rocks. Rock Mech Rock Eng 47:1165–1181. https://doi.org/10.1007/s00603-013-0451-2
33. Hatzor YH, Palchik V (1997) The influence of grain size and porosity on crack initiation stress and critical flaw length in dolomites. Int J Rock Mech Min Sci 34(5):805–816. https://doi.org/10.1016/S1365-1609(96)00066-6
34. Eberhardt E, Stimpson B, Stead D (1999) Effects of grain size on the initiation and propagation thresholds of stress-induced brittle fractures. Rock Mech Rock Eng 32:81–99. https://doi.org/10.1007/s006030050026
35. Backers T, Stephansson O (2012) ISRM suggested method for the determination of Mode II fracture toughness. Rock Mech Rock Eng 45:1011–1022. https://doi.org/10.1007/s00603-012-0271-9
36. Haeri H, Shahriar K, Marji MF, Moarefvand P (2014) On the strength and crack propagation process of the pre-cracked rock-like specimens under uniaxial compression. Strength Mater 46(1):140–152. https://doi.org/10.1007/s11223-014-9525-y
37. Bartmann K, Alber M (2017) Experimental determination of crack Initiation and crack damage of two granites. Proc Eng 191:119–126. https://doi.org/10.1016/j.proeng.2017.05.162
38. Kong R, Feng XT, Zhang X, Yang C (2018) Study on crack initiation and damage stress in sandstone under true triaxial compression. Int J Rock Mech Min Sci 106:117–123. https://doi.org/10.1016/j.ijrmms.2018.04.019
39. Ning J, Wang J, Jiang J, Hu S, Jiang L, Liu X (2018) Estimation of crack initiation and propagation thresholds of confined brittle coal specimens based on energy dissipation theory. Rock Mech Rock Eng 51:119–134. https://doi.org/10.1007/s00603-017-1317-9
40. ISRM (2007) The complete ISRM suggested methods for rock characterization, testing and monitoring: 1974–2006. In: Ulusay R, Hudson JA (eds) Suggested methods prepared by the commission on testing methods. 2007 International Society for Rock Mechanics (ISRM), Ankara, Turkey
41. Pengfei L, Qingchi C (2014) Analysis of the approaches to determine crack initiation stress of rock materials in compression tests. Appl Mech Mater 556–562:2857–2861. https://doi.org/10.4028/www.scientific.net/AMM.556-562.2857
42. Folk RL (1981) Petrology of sedimentary rocks, Hemphill Pub., Austin. ISBN: 0-914696-14-9
43. Folk RL, Ward WC (1957) Brazos River bar, a study in the significance of grain size parameters. J Sediment Petrol 27(1):3–26. https://doi.org/10.1306/74D70646-2B21-11D7-8648000102C1865D
44. Wong RHC, Chau KT, Wang P (1996) Microcracking and grain size effect in Yuen Long Marbles. Int J Rock Mech Min Sci Geomech Abstr 33(5):479–485. https://doi.org/10.1016/0148-9062(96)00007-1
45. Tugrul A, Zarif IH (1999) Correlation of mineralogical and textural characteristics with engineering properties of selected granitic rocks from Turkey. Eng Geol 51:303–317. https://doi.org/10.1016/S0013-7952(98)00071-4
46. Přikryl R (2001) Some microstructural aspects of strength variation in rocks. Int J Rock Mech Min Sci 38(5):671–682. https://doi.org/10.1016/S1365-1609(01)00031-4
47. Bieniawski ZT (1989) Engineering rock mass classifications: a complete manual for engineers and geologists in mining, civil and petroleum engineering. Wiley-Interscience, New York
48. Barton N (1988) Rock mass classification and tunnel reinforcement selection using the Q system. In: Kirkaldie L (ed) Rock classification systems for engineering purposes, ASTM STP 984. American Society for Testing Materials, pp 69–88. https://doi.org/10.1520/STP984-EB
49. Gerçek H (1986) Stability considerations for underground excavation intersections. Min Sci Technol 4(1):49–57. https://doi.org/10.1016/S0167-9031(86)90194-5